

2020

Synthesis of new molybdenum perfluoropinacolate complexes and investigation of CuSn alloys for nitrate reduction

<https://hdl.handle.net/2144/40942>

"Downloaded from OpenBU. Boston University's institutional repository."

BOSTON UNIVERSITY
COLLEGE OF ENGINEERING

Thesis

**SYNTHESIS OF NEW MOLYBDENUM PERFLUOROPINACOLATE
COMPLEXES AND INVESTIGATION OF CuSn ALLOYS
FOR NITRATE REDUCTION**

by

SIKYUNG CHOI

Pharm.D., Massachusetts College of Pharmacy and Health Sciences, 2012

Submitted in partial fulfillment of the
requirements for the degree of
Master of Science

2020

Approved by

First Reader

Linda H. Doerrer, Ph.D.
Associate Professor of Chemistry
Associate Professor of Materials Science and Engineering

Second Reader

Sean J. Elliott, Ph.D.
Professor of Chemistry
Professor of Materials Science and Engineering

Acknowledgements

Pursuing a new degree after years of non-academic life has been a challenge. Towards the end of my graduate program at Boston University, I am glad I did take the risk. I have learned a great deal about the area of science that interest me. Moreover, I learned valuable life lessons over the time I spent working towards the thesis and the degree.

I would like to thank my advisor, Professor Linda H. Doerrer. Her guidance directed me to handle problems and achieve goals I otherwise would have thought to be impossible. She is a great teacher and helped me tremendously through times of hardship. I am motivated to move forward thanks to her wisdom and kindness. I am grateful to have been a member of the Doerrer group. I also would like to thank the Whitty group who graciously allowed me to use their equipment.

I thank everyone in the Doerrer group: Dr. Nate Hartmann, Dr. Sarah Neville Brazeau, Sarah Beach Molony, Jessica Elinburg, Léa Toubiana, Shawn Moore, Hannah Skipper, Linda Zuckerman, Claire May, Nichakan Khuichad, Paul Homuth, Ana Herring. Everyone took time to help me get used to a research setting and laboratory equipment. I initially knew nothing and had to be taught every step of how to conduct an experiment. I thank the group members for their patience and eagerness to help me. I was fortunate to work on the same project as Nate and Léa and I have learned from their assistance which made my work possible.

My friends from the Material Science and Engineering program: Vicky Luan, Brian Pihuleac, Jason Lucas, we went through fun yet tough times together. Thank you for your support. I have no idea how I could have completed the program without you all.

And lastly, I thank my family: Mom, dad, my sister Shawn for their sacrifice and trust that made me pursue this degree. They believed in me wholeheartedly and helped

me overcome times of hardship. I will be eternally grateful to them.

**SYNTHESIS OF NEW MOLYBDENUM PERFLUOROPINACOLATE
COMPLEXES AND INVESTIGATION OF CuSn ALLOYS
FOR NITRATE REDUCTION**

SIKYUNG CHOI

ABSTRACT

1. Synthesis of New Molybdenum Perfluoropinacolate Complexes

Fluorinated alkoxide ligands, including perfluoropinacol ($\text{H}_2\text{pin}^{\text{F}}$), have been investigated for their ability to support high oxidation status for $3d$ transition metals. Molybdenum is a $4d$ transition metal used for its catalytic effect in nature as well as in industry. Three new Mo pin^F-containing anions $[\text{MoO}_3(\text{pin}^{\text{F}})]^{2-}$, $[\text{Mo}_2\text{O}_4(\mu_2\text{-O})(\text{pin}^{\text{F}})_2]^{2-}$, $[\text{Mo}_2\text{O}_2(\mu\text{-O})_2(\text{pin}^{\text{F}})_2]^{2-}$ have been synthesized and structurally characterized. The pin^F ligands have been found to stabilize both monomeric and dimeric Mo(V) complexes and a dimeric Mo(VI) complex. These compounds can be further studied to look for catalytic redox reactions, and for potential understanding of the rates and mechanism of catalysis.

2. Investigation of CuSn Alloys for Nitrate Reduction

Algal blooms are environmentally hazardous phenomena that cause major damage to aquatic ecosystems. One factor responsible for this effect is the overuse of nitrogen-based fertilizers that has led to accumulation of nitrate (NO_3^-) in open waters. Nitrate is a nutrient for algae, and when algae proliferate too quickly it causes hypoxia of water. Cu is a well-known catalyst for the electrocatalytic reduction of NO_3^- and Sn is known to promote selectivity for N_2 as the final product of NO_3^- reduction. The catalytic effect of CuSn alloys for the reduction of nitrate and nitrite have been studied to find the optimum Cu to Sn ratio for this application. It was found that a ratio of 1:1 resulted in the highest peak catalytic

current but still less than pure Cu. Additionally, deposition methods on a glassy carbon electrode (GCE) were optimized. It was found that Cu-Sn co-deposition on GCE by controlled potential electrolysis (CPE) was found to be most stable when surfactant K_3 citrate was added to the deposition solution. Analysis of the final products of NO_3^- reduction through a microcolorimetric assay was inconclusive and requires further optimization to obtain meaningful data.

Table of Contents

1. Synthesis and Characterization of New Molybdenum Perfluoropinacolate Complexes	1
1.1 Introduction	2
1.1.1 Fluorinated Ligands.....	2
1.1.2 Molybdenum	3
1.1.3 Characterization Techniques	3
1.2 Experimental	4
1.2.1 General Procedure.....	4
1.2.3 X-ray Crystallography.....	9
1.2.4 Electrochemistry.....	9
1.3 Results and Discussion	10
1.3.1 X-ray Crystallography.....	10
1.3.2 NMR Spectroscopy	15
1.3.3 Electrochemistry.....	17
1.4 Conclusions and Future Directions	18
2. Investigation of CuSn Alloys for Nitrate Reduction Catalysis	20
2.1 Introduction	21
2.2 Experimental	22
2.2.1 General Procedures	22
2.2.2 Linear Sweep Voltammetry (LSV).....	23
2.2.3 Cyclic Voltammetry (CV).....	23
2.2.4 Controlled Potential Electrolysis (CPE).....	24
2.2.5 Microcolorimetric Assay	24
2.3 Results and discussion	25
2.3.1 Linear Sweep Voltammetry	25
2.3.2 Cyclic Voltammetry	28
2.3.3 Microcolorimetric Assay	32
2.4 Conclusions and Future Directions	32
References	34
Curriculum Vitae	38

List of Tables

Table 1.1. Selected Metrical Parameters for Complexes I – IV	12
Table 2.1. Potential of Reduction Peak of NO_3^- Reduction and Current at -1.2V Based on Cu Sn Ratio.....	29

List of Figures

Figure 1.1. Synthesis of $(\text{NH}_4)_2[\text{MoO}_4]$	5
Figure 1.2. Synthesis of $(\text{Et}_3\text{NH}_4)_2[\text{MoO}_4]$	5
Figure 1.3. Protonolysis of $(\text{NH}_4)_2[\text{MoO}_4]$ with $\text{H}_2\text{pin}^{\text{F}}$	6
Figure 1.4. Syntheses of $(\text{Et}_3\text{NH})_2[\text{Mo}(\text{O})_3(\text{pin}^{\text{F}})]$ (II) and $(\text{Et}_3\text{NH})_2[\text{Mo}_2(\text{O})_4(\mu_2\text{-O})(\text{pin}^{\text{F}})_2]$ (III).....	8
Figure 1.5. Reduction of $(\text{Et}_3\text{NH})_2[\text{Mo}(\text{O})_3(\text{pin}^{\text{F}})]$ (II) and $(\text{Et}_3\text{NH})_2[\text{Mo}_2(\text{O})_2(\mu_2\text{-O})(\text{pin}^{\text{F}})_2]$ (III) to yield $(\text{Et}_3\text{NH})_2[\text{Mo}_2\text{O}_2(\mu\text{-O})_2(\text{pin}^{\text{F}})_2]$ (IV).....	9
Figure 1.6. ORTEP drawings of anions of II , III , and IV . Ellipsoids shown at the 50% level. Counter cations and solvent molecules omitted for clarity.....	11
Figure 1.7. Structure of $[\text{Mo}_3\text{O}_8(\text{C}_6\text{H}_{12}\text{O}_2)_2]$	12
Figure 1.8. ^{19}F -NMR spectrum of I in CD_3CN	16
Figure 1.9. ^1H -NMR spectrum of I in CD_3CN	17
Figure 1.10. Cyclic Voltammetry of (a) 3.1mM $[\text{TAA}][\text{DAAM}][\text{MoO}_3\text{Pin}^{\text{F}}]$ with 0.25M NtBu_4PF_6 as the supporting electrolyte in CH_3CN (b) 0.25M NtBu_4PF_6 in CH_3CN	18
Figure 2.1. LSV in 50mM KCl of metal on GCE deposited from 1M HCl 10mM CuCl_2 10mM SnCl_2	27
Figure 2.2. LSV in 50mM KCl of metal on GCE deposited from (a)1M H_2SO_4 10mM CuCl_2 10mM SnCl_2 while stirring for 1 min, (b) 1M H_2SO_4 10mM CuCl_2 10mM SnCl_2 30mM $\text{K}_3\text{citrate}$ while stirring for 1 min.....	28
Figure 2.3. CV in 50mM KCl 50mM KNO_3 of NO_3^- reduction catalysis by metal deposited from 1M H_2SO_4 while stirring for 1 min and (a)10mM SnCl_2 (Cu:Sn Ratio 0:1) (b) 10mM CuCl_2 5mM SnCl_2 (2:1) (c) 10mM CuCl_2 7.5mM SnCl_2 (4:3) (d) 10mM CuCl_2 10mM SnCl_2 (1:1) (e) 10mM CuCl_2 (1:0).....	29
Figure 2.4. SEM image of GCE surface with Cu Sn deposition.....	30
Figure 2.5. SEM image of GCE surface with Cu Sn deposition with $\text{K}_3\text{citrate}$	31

1. Synthesis and Characterization of New Molybdenum Perfluoropinacolate Complexes

1.1 Introduction

1.1.1 Fluorinated Ligands

The field of coordination chemistry has studied metal complexes with alkoxide ligands in order to synthesize new catalysts. Alkoxides are a good candidate for this application as they make strong bonds with metals. Alkoxide-metal complexes are also of interest because they can act as precursors of metal oxides.^{1,2} However, transition metal alkoxide complexes have low hydrolytic stability, which means the application of alkoxide-metal complexes can be limited. Fluorinated alkoxides provide a solution to the low stability problem. Fluorine atoms on a carbon withdraw electrons to the point that the adjacent metal-oxygen bond is less easily protonated. Therefore, the fluorinated alkoxide metal complexes are more stable at high oxidation states and the ligand is less likely to be involved in bridging. Perfluoropinacol ($\text{H}_2\text{pin}^{\text{F}}$) is one example of a fluorinated O-donor ligand that has been studied before on 3d metals in high oxidation states.^{3,4}

The Doerrer group has focused on the synthesis of first-row transition metals supported by fluorinated O-donor ligands including $\text{H}_2\text{pin}^{\text{F}}$. Many 3d metal- pin^{F} complexes have been studied as catalysts for various reactions. One example is the vanadium complex, $[\text{V}_2(\text{O})_2(\mu\text{-O})_2(\text{pin}^{\text{F}})_2]^{2-}$, that has been studied as a catalyst for oxidative alcohol dehydrogenation activity.⁵ With much of the spectrum of 3d transition metals, Mn, Fe, Co, Ni, Cu, and Zn explored in past works; new attention was turned toward attempting 4d metals for metal- pin^{F} complexes.⁶⁻⁹

1.1.2 Molybdenum

Molybdenum is a 4d metal in group 6 historically used as an alloy element for its high melting point and durability. One famous use of molybdenum is as an additive to steel used in the manufacture of automobiles.¹⁰ In biology, molybdenum is a cofactor in various enzymes including sulfite oxidase, xanthine oxidase, and aldehyde oxidase. It acts as a reducing agent to sustain a functioning physiology in living organisms.¹¹ Molybdenum compounds in inorganic chemistry have been well studied in order to create catalysts with similar activity. Additionally, molybdenum disulfide is a well-known component in catalysts for hydrodesulfurization of petroleum.¹² Use of molybdenum alkoxide complexes as catalysts for the oxidation of alkenes to epoxides have also been reported.^{13–15}

1.1.3 Characterization Techniques

X-ray Crystallography. X-rays with very short wavelengths (λ) diffract through a single crystal and display a distinct and unique pattern. The nature of the crystalline lattice gives rise to regular repeated patterns that intensify the diffracted signal through constructive and destructive interference. This pattern allows the determination of the positions, arrangements and spacing of atoms in the lattice.¹⁶ The angle of diffraction (θ) is proportional to the distance (d) of the lattice spacing in a crystal and the relationship is given by Bragg's law (Equation 1.1):

$$\lambda = 2 d \sin \theta \qquad \text{Eq. 1.1}$$

Nuclear Magnetic Resonance (NMR) Spectroscopy. NMR spectroscopy is a method of analyzing a chemical structure by measuring radio signals from atoms in a strong magnetic field perturbed by an applied radio frequency. Atoms with an odd number of

protons or neutrons have a nuclear spin state (I) of e.g. $\pm\frac{1}{2}, \pm\frac{3}{2}, \pm\frac{5}{2}, \pm\frac{7}{2}$, etc..., with the sign indicating the orientation with respect to a magnetic field. An atom of interest in a chemical sample under analysis in an applied magnetic field can change its spin direction with the energy it receives from the radio frequency. The frequency that allows + and – states to be in equilibrium is the resonance frequency. The energy difference between the atoms at opposite spin states, or also referred to as the energy absorption line, is found by equation 1.2:

$$\Delta E = h\nu = -\gamma\hbar H \quad \text{Eq. 1.2}$$

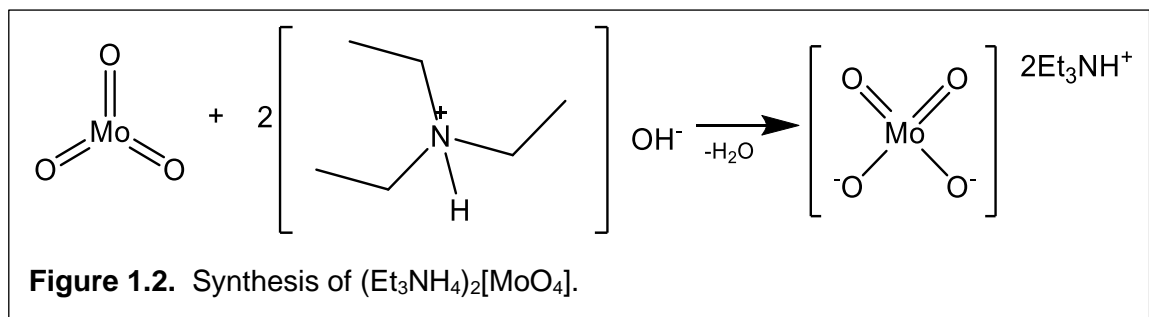
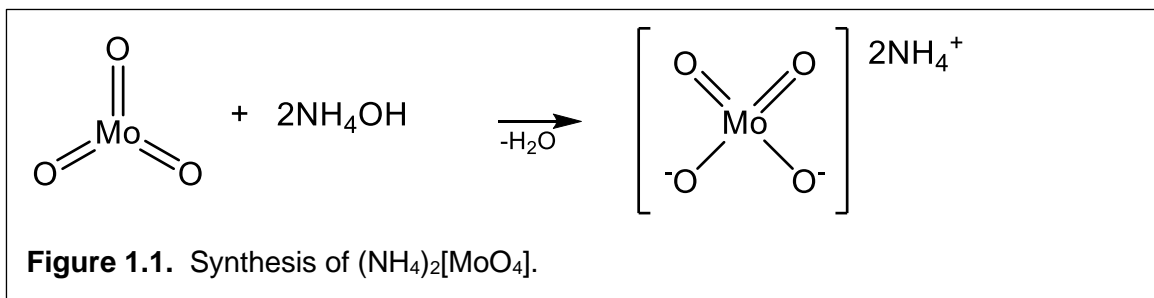
The energy absorption line occurs at a different frequency (chemical shift) depending on the electronic environment an atom is in.¹⁷

1.2 Experimental

1.2.1 General Procedure

All Mo(V) and Mo(VI) complexes were prepared in air under ambient conditions. Deionized H₂O, and EtOH were used as solvents for aerobic syntheses. Acetonitrile (CH₃CN) was used for electrochemistry. ¹H and ¹⁹F NMR samples were prepared in air using CD₃CN as a solvent. NMR spectra were measured using a Varian 500 MHz spectrometer. Chemical shifts (δ) for ¹H NMR spectra were referenced to the resonance of residual protio solvent, and chemical shifts for ¹⁹F NMR were referenced to trichlorofluoromethane (CCl₃F). Molybdenum trioxide (MoO₃) and H₂pin^F are commercially available and used as received. Ammonium hydroxide (NH₄OH) 30% was diluted in deionized water to make a stock solution of 1 M concentration.

Molybdenum starting materials. Molybdenum trioxide (MoO_3) is stable in air at room temperature but is insoluble in water making it challenging to use synthetically. However, the molybdate ion (MoO_4^{2-}) is soluble, and therefore is a convenient Mo(VI) starting material. Conversion of MoO_3 to MoO_4^{2-} in an aqueous environment is assisted with the presence of a base.¹⁸ The two amines selected to create a basic aqueous solution were ammonia (NH_3 , Figure 1.1) and triethylamine (Et_3N , Figure 1.2). Both are readily available and have boiling points lower than water ($-33.34\text{ }^\circ\text{C}$ and $89\text{ }^\circ\text{C}$, respectively). This feature makes removal of excess base possible via evaporation following the synthesis of MoO_4^{2-} .



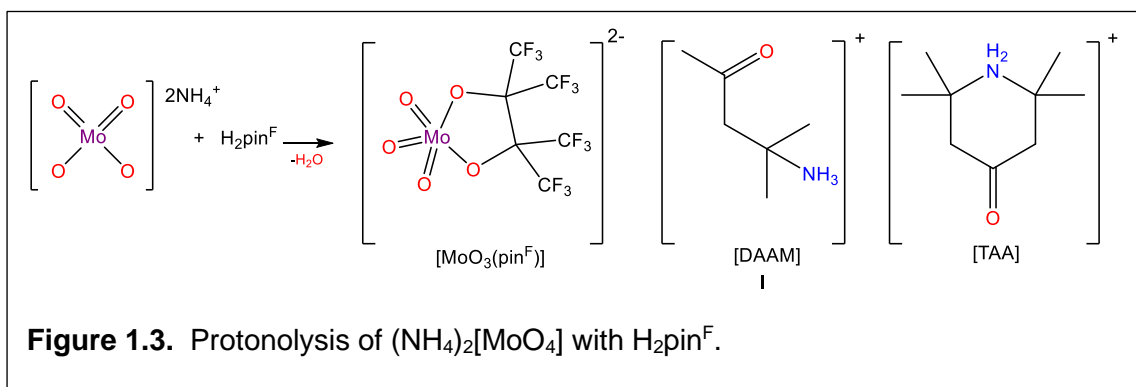
MoO_3 dissolves in an aqueous solution that has 5 times the amount of ammonium hydroxide (NH_4OH , the dissolved form of ammonia in water,) or triethylammonium hydroxide ($(\text{Et}_3\text{NH})\text{OH}$, hydrated Et_3N). Therefore excess ammonia or amine remaining after the completion of the reaction with $\text{H}_2\text{pin}^{\text{F}}$ is guaranteed and must be removed.

Perfluoropinacol. The process of dissolving perfluoropinacol ($\text{H}_2\text{pin}^{\text{F}}$) in polar solvents such as water or ethanol is highly exothermic with the risk of inducing self-evaporation. Some of the $\text{H}_2\text{pin}^{\text{F}}$ is expected to be lost in the process of dilution of pure $\text{H}_2\text{pin}^{\text{F}}$. The pK_{a} values of the two protons in $\text{H}_2\text{pin}^{\text{F}}$ are 6.0 and 10.7.⁴ Both protons are likely to leave when $\text{H}_2\text{pin}^{\text{F}}$ in a basic environment with $\text{pH} > 11$.

1.2.2 Synthetic Procedure

Synthesis of Triacetan ammonium (TAA) Diacetone ammonium (DAAM) [$\text{MoO}_3 \text{pin}^{\text{F}}$] (I)

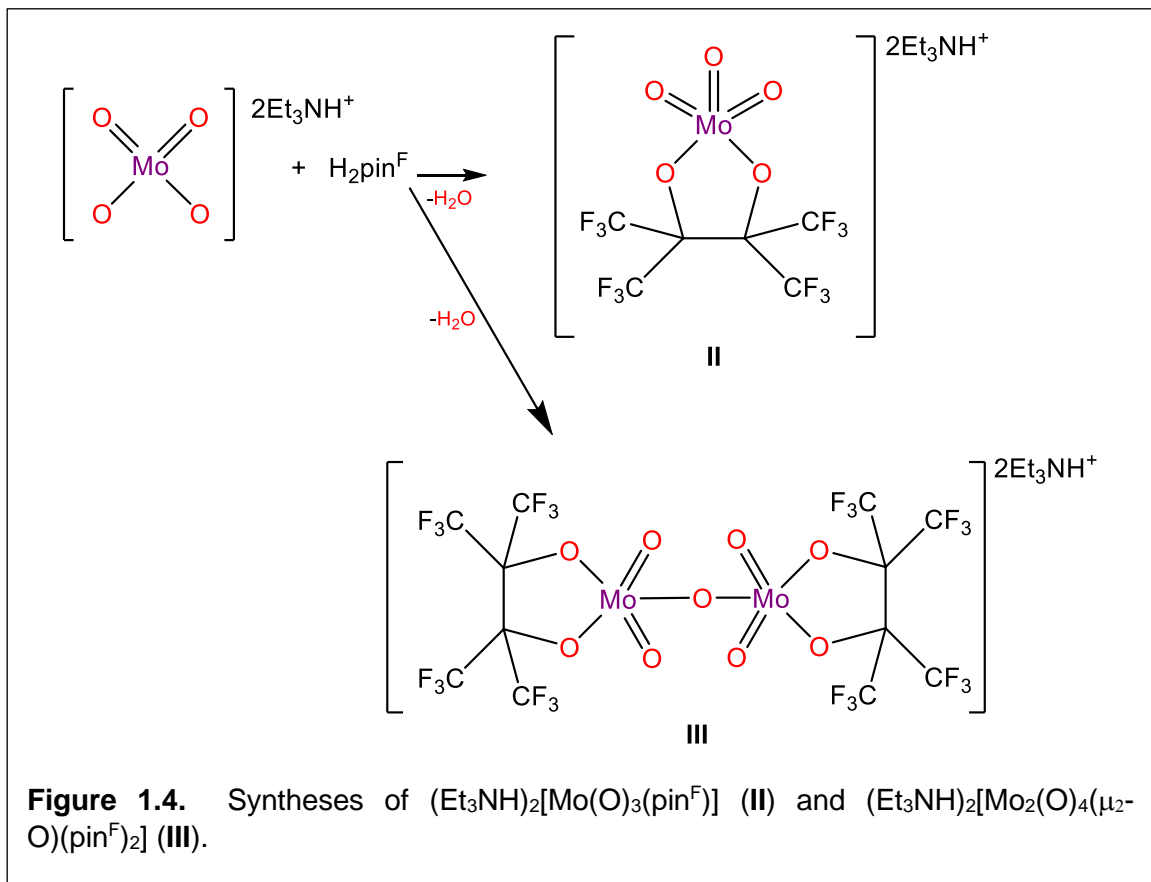
MoO_3 (0.4122g, 3mmol) is dissolved in 12mL 1M NH_4OH in water and becomes a clear colorless solution of ammonium molybdate ($(\text{NH}_4)_2\text{MoO}_4$). Meanwhile, $\text{H}_2\text{pin}^{\text{F}}$ (1g, 3mmol) is dissolved in 5mL of ethanol (EtOH). The process of dissolving $\text{H}_2\text{pin}^{\text{F}}$ is exothermic enough to evaporate $\text{H}_2\text{pin}^{\text{F}}$ itself. Consequently, $\text{H}_2\text{pin}^{\text{F}}$ is gradually added to a vial containing EtOH while the vial cap is held to cover most of the vial opening to prevent $\text{H}_2\text{pin}^{\text{F}}$ escaping via evaporation. Subsequently, the molybdate solution was added to the solution of $\text{H}_2\text{pin}^{\text{F}}$ in ethanol and allowed to stir overnight then dried under vacuum to yield [DAAM] [TAA] [$\text{MoO}_3 \text{pin}^{\text{F}}$]. Colorless crystals are obtained by slow evaporation with acetone and chloroform.



Yield is not available due to the crystals being used for X-ray characterization.

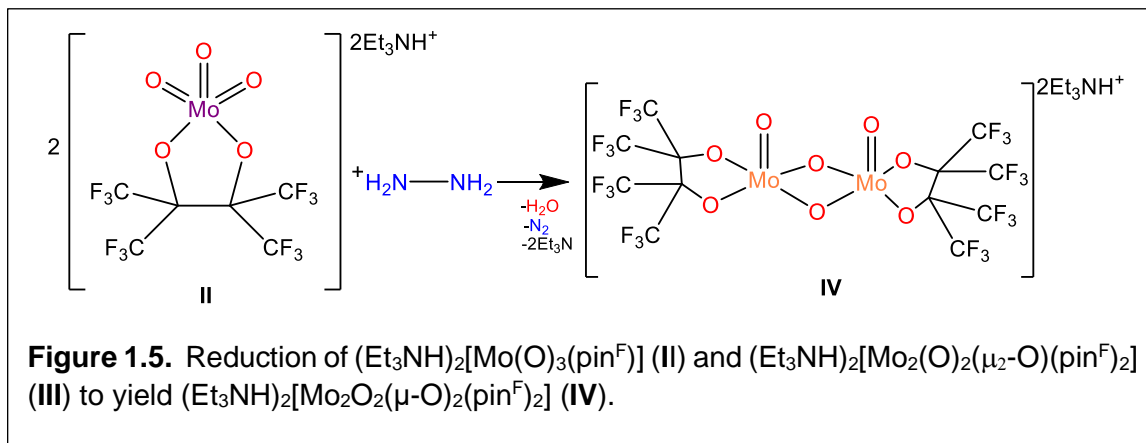
Synthesis of $(Et_3NH)_2[MoO_3(pin^F)]$ (II) and $(Et_3NH)_2[Mo_2O_4(\mu_2-O)(pin^F)_2]$ (III)

MoO_3 (0.5784g, 4mmol) was dissolved in 35mL of water and 2.5mL of Et_3N to form triethylammonium molybdate ($(Et_3NH)_2MoO_4$). As in the process of synthesizing complex I, H_2pin^F (1.3686g, 4mmol) is dissolved in 5mL of EtOH. The solution of $(Et_3NH)_2MoO_4$ was added to the H_2pin^F in EtOH and allowed to stir overnight. Volatiles were removed from the resulting solution *in vacuo* to yield a pale yellow-green amorphous solid (1.7655g, 69.6% crude yield). Colorless crystals of II and III were obtained by slow evaporation with dichloromethane (DCM) and methyl tert-butyl ether (MTBE). Crystalline yield is unavailable due to the crystals being used for X-ray characterization.



Synthesis of $(\text{Et}_3\text{NH})_2[\text{Mo}_2\text{O}_2(\mu\text{-O})_2(\text{pin}^{\text{F}})_2]$ (IV)

Complex **IV** is synthesized by the addition of hydrazine monohydrate (0.041g, 0.8mmol) to a mixture of **II** and **III** (2.5455g) dissolved in 5mL of EtOH and allowed to stir overnight. Volatiles were removed from the resulting solution *in vacuo* to yield an orange amorphous solid (0.7772g, 56.8% crude yield). Yellow crystals were obtained via slow evaporation with MTBE and hexane. Crystalline yield is unavailable as this material was used for X-ray characterization.



1.2.3 X-ray Crystallography

Crystal data for all complexes were collected by the Rheingold group at UCSD on Bruker diffractometers equipped with either an APEX-CCD or CMOS detector with $\text{Mo}(K\alpha)$ radiation ($\lambda = 0.71073 \text{ \AA}$). All obtained data were corrected for absorption using the SADABS program. All structures were solved by heavy-atom methods and the remaining non-hydrogen atoms were located from subsequent difference maps. All structures were refined with anisotropic thermal parameters for all non-hydrogen atoms; hydrogen atoms were treated as idealized contributions. The high residual R value is suggestive of additional disorder, but no attempt was made to address this point. The refinement of F^2 was calculated against all reflections.

1.2.4 Electrochemistry

Cyclic voltammetry studies of **I** were performed in CH_3CN using 3.1 mM of **I** and 0.25 M TBAPF_6 (tetra-*n*-butylammonium hexafluorophosphate) as the supporting electrolyte under open air using a three-electrode cell connected to an external CHI 630C potentiostat run by a personal computer with CHI software. A glassy carbon electrode (0.5 mm

diameter) was employed as the working electrode, with Ag/AgCl or Ag wire (quasi)electrode as the reference and Pt wire as the counter electrode, respectively. The sample was degassed with N₂ gas for 10 min prior to running a cyclic voltammogram. The working electrode was polished between experiments using 5 μm Al₂O₃ suspended in water and then carefully dried. Voltammograms were recorded with 100mV/s scan rate and all potentials are reported *versus* [Ag]⁺/[AgCl].

1.3 Results and Discussion

1.3.1 X-ray Crystallography

Four new Mo-containing compounds have been structurally characterized, and the ORTEPs of three Mo-containing anions are shown in Figure 1.6. Crystallography data for **I**, **II**, **III**, and **IV** show that the coordination number of the molybdenum atom is five in all cases. Surprisingly, only one oxygen atom in [MoO₄]²⁻ is displaced by pin^F. Compared to other transition metal-pin^F complexes, the Mo centers in **I**, **II**, **III**, **IV** are bound to only one pin^F ligand. Previous work with 3d metals has demonstrated numerous examples of binding to two pin^F ligands as a monomer, {M(pin^F)₂}, as well as coordination to one pin^F ligand to each metal in an oxo-bridged dimer, {(pin^F)M-O-M(pin^F)}. The structures of compounds **II**, **III**, and **IV** were obtained through X-ray crystallography and a summary of key bond lengths and the structural parameter τ_5 is given in Table 1.1.

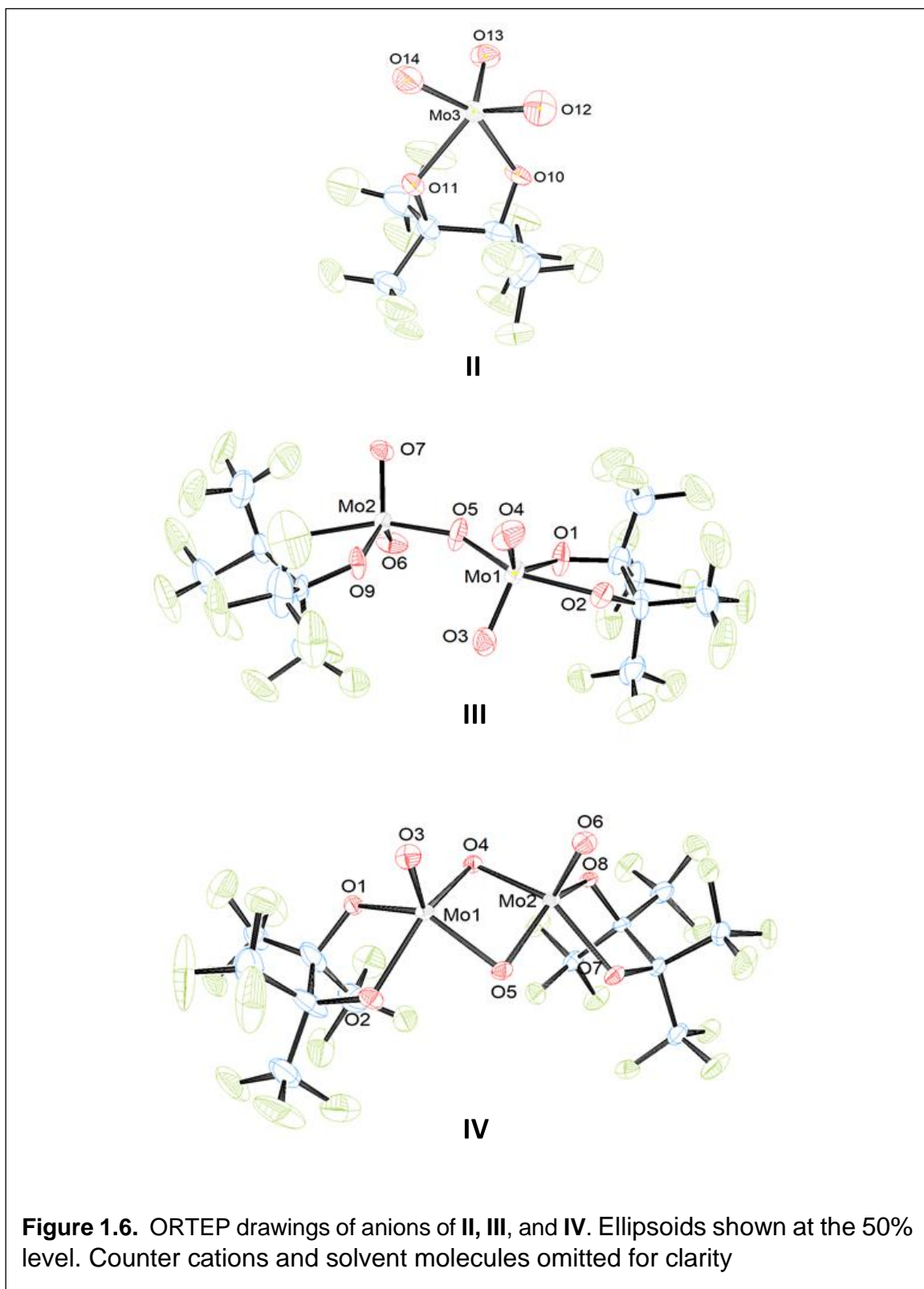
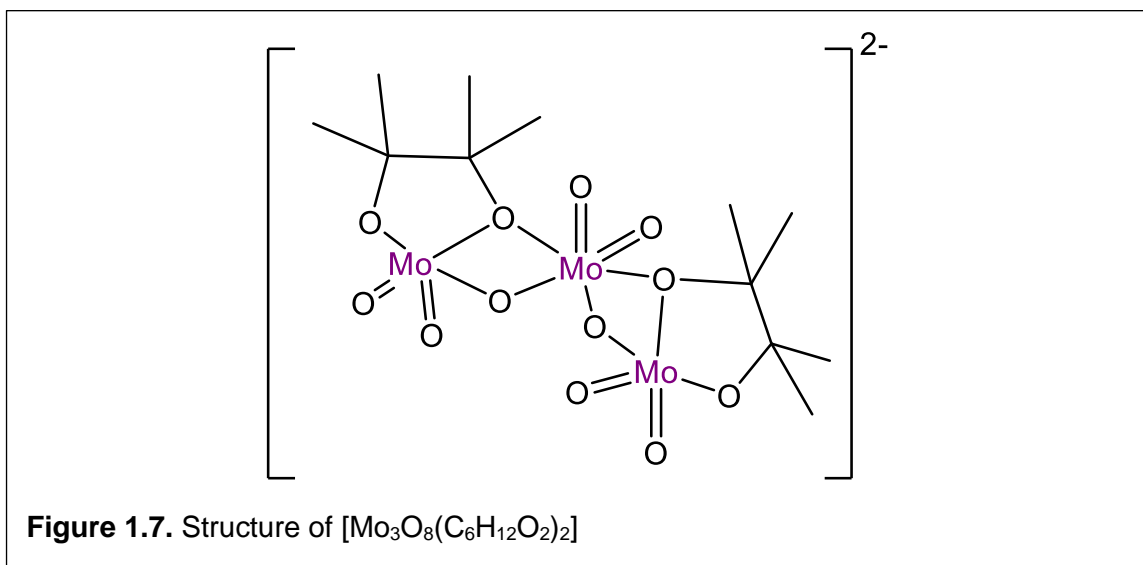


Figure 1.6. ORTEP drawings of anions of **II**, **III**, and **IV**. Ellipsoids shown at the 50% level. Counter cations and solvent molecules omitted for clarity

Table 1.1. Selected Metrical Parameters for Complexes I – IV

	I	II	III	IV	
Selected Bond Lengths(Å)	Mo=O	1.764(2)	1.729(10)	1.681(9)	1.677(4)
		1.745(2)	1.716(9)	1.699(8)	
		1.722(2)	1.758(8)		
Mo-O(pin ^F)	2.096(2)	2.069(7)	2.028(8)	2.017(4)	
	2.054(2)	2.074(7)	2.043(8)	2.010(4)	
Mo-O(μ-O)			1.877(9)	1.954(4)	
				1.942(4)	
Structural Parameter	τ_5	0.33	0.46	0.36	0.076

Compounds **III** and **IV** show a common feature of fluorinated alkoxide ligands in that [pin^F] itself does not participate in bridging the two molybdenum atoms. In contrast, bridging by a non-fluorinated pinacolate ligand was seen in



$[\text{Mo}_3\text{O}_8(\text{C}_6\text{H}_{12}\text{O}_2)_2]^{2-}$ (Fig. 1.7) as reported by Chen, Ma, Liu, and Zubieta.¹⁹ In this structure, an oxygen atom from a pinacolate bridges two separate molybdenum atoms. With this non-fluorinated form of pinacolate, the oxygen atom is much more Lewis basic and has enough electron density to become a strong donor. Whereas in the cases of **III** and **IV**, the bridging oxygen atoms linking the two distinct molybdenum atoms do not bond to anything else since the fluorine atoms withdraw electrons away from the oxygen atoms making them weaker donors. Therefore, the oxygen atoms on pin^F do not participate in bridging to another molybdenum. This pattern has been seen in other comparisons between fluorinated and non-fluorinated alkoxide ligands.²⁰

The numbers and lengths of Mo-O bonds around each Mo atom are of interest due to the consistent pattern seen with a comparable structure of $\text{Mo}_2(\text{C}_6\text{H}_{12}\text{O}_2)_2(\text{C}_6\text{H}_{13}\text{O}_2)_2\text{O}_3$ synthesized by Matheson and Penfold and the previously mentioned $\text{Mo}_3\text{O}_8(\text{C}_6\text{H}_{12}\text{O}_2)_2$.^{19,21} In the $\text{Mo}_2(\text{C}_6\text{H}_{12}\text{O}_2)_2(\text{C}_6\text{H}_{13}\text{O}_2)_2\text{O}_3$ structure, which has a coordination number of six, the bond length between molybdenum and the terminal oxo group (Mo=O) is the shortest (1.67 Å) compared to the bonds that molybdenum makes with other oxygen atoms Mo-O pinacol bonds (1.86 - 2.34 Å) and the Mo-O μ -oxo bonds (1.90 Å). In $\text{Mo}_3\text{O}_8(\text{C}_6\text{H}_{12}\text{O}_2)_2$, the Mo=O bond lengths (1.712 Å, 1.696 Å) are shorter than that of Mo-O pinacol bonds (1.944 Å, 2.038 Å) and the Mo-O μ -oxo bond (1.915 Å).

Table 1.2. Selected Bond Lengths (Å) for Literature {MoO_n} Environments

	Mo₂(C₆H₁₂O₂)₂(C₆H₁₃O₂)₂O₃	Mo₃O₈(C₆H₁₂O₂)₂
Mo=O	1.67(1)	1.696(8) 1.712(8)
Mo-O(pinacolate)	2.34(1)	1.944(8)
	1.86(1) 1.98(1) 1.89(1)	2.038(7)
Mo-O(μ-O)	1.90(1)	1.915(7)

The same trend is seen in complexes **I**, **II**, **III**, and **IV** (**Table 1.1**). The terminal oxo bonds are the shortest among the three types of bonds. In the cases of **III** and **IV**, the bridging μ-O bonds with molybdenum are the next shortest. In all cases, the bond lengths between molybdenum and oxygen in the pin^F ligand are the longest which is consistent with non-fluorinated ligand complexes of Mo.

Surprisingly, the structure of **I** shows that the counter cations of **I** are diacetoneammonium (DAAM) and 2,2,6,6-Tetramethyl-4-piperidinium (triacetonammonium, TAA). These organic cations are the result of an acetone and ammonia condensation reaction. The NH₄⁺ ion from the preparation of MoO₄²⁻ is likely to act as a weak Brønsted acid and catalyse the condensation reaction.²² This condensation reaction is proposed as the reason why crystals were easier to obtain. TAA and DAAM possibly have better packing properties than NH₄⁺ ion. The cations TAA and DAAM are bulkier than NH₄⁺ which makes crystal packing easier in all three dimensions. Crystals of **II**, **III** and **IV** are big enough for X-ray diffraction for the same reason. [Et₃NH]⁺ is bulky

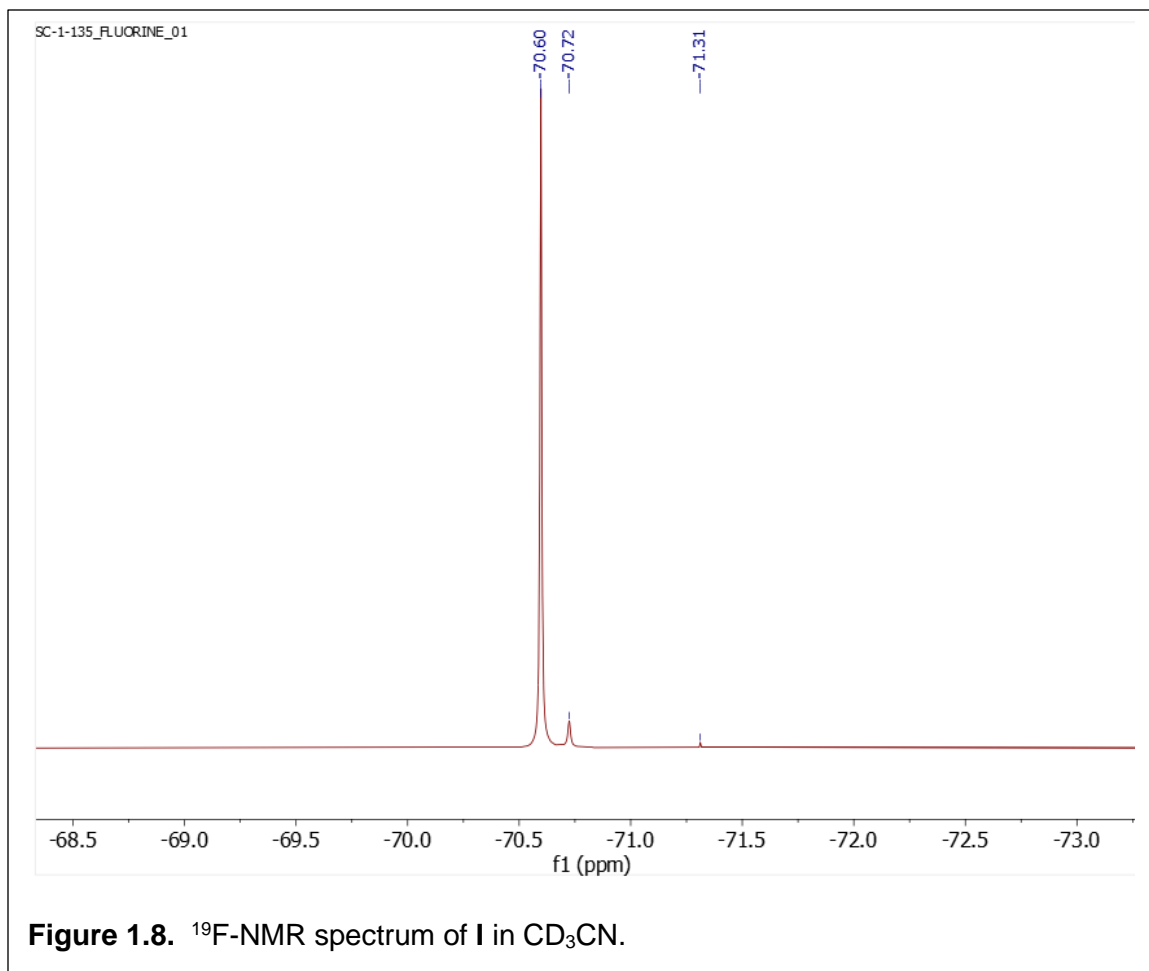
enough for easy crystal packing in all dimensions.

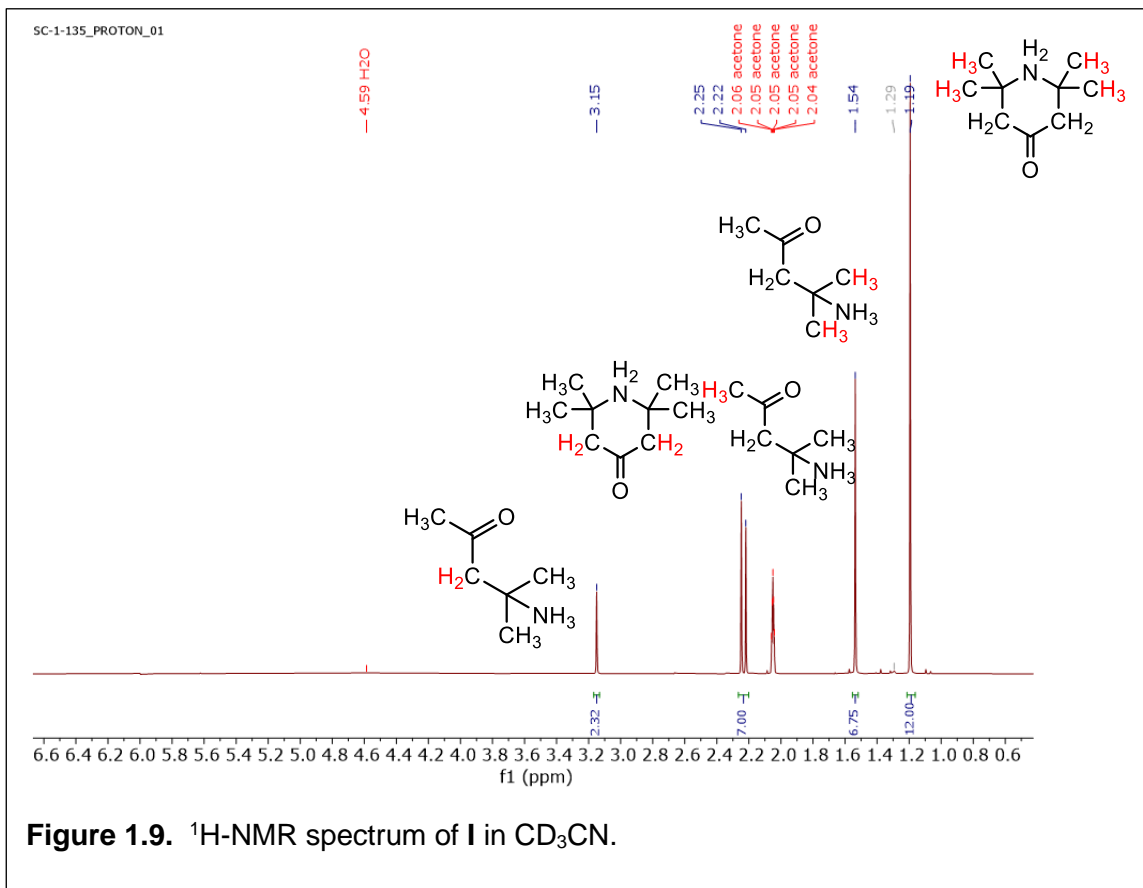
Complexes **II** and **III** co-crystallized from a single reaction that used Et₃N as the base to dissolve MoO₃, whereas starting with NH₄OH resulted in only a single product **I**. The choice of base used in synthesis is significant. The conditions that only favor exclusively **II** or exclusively **III** are yet to be discovered.

The τ_5 values of **I**, **II**, **III** are at least four times of that of **IV**. As τ_5 approaches 1, the geometric shape of a five-coordinate complex is more trigonal bipyramidal and as τ_5 approaches 0 the shape is more square pyramidal. Mo(V) tends more towards a square pyramidal shape than Mo(VI). In **IV**, the two Mo=O bonds are in *cis* positions to each other. Steric hindrance from oxygen is less of a factor in determining the geometry.

1.3.2 NMR Spectroscopy

¹⁹F NMR and ¹H NMR spectra were collected for complex **I**. The ¹⁹F NMR spectrum (Fig 1.8) displays a single prominent peak which is indicative of an acceptably pure product with all fluorine atoms in the same chemical environment. ¹H NMR spectroscopy reveals hydrogen atoms on the counter cations in **I**, DAA and TAA, as well as trace amounts of water and acetone which were solvents used during synthesis and crystallization (Fig. 1.9). Excluding the peaks from the solvents, the integration values for each of the five peaks correspond to the number of hydrogens bonded to carbons in the same type of bonds. The accordance of the integrated sums with the number of hydrogens in a certain C-H bond is another indicator of the purity of the obtained crystals of **I** and that the catalytic effect of NH₄⁺ is very selective for the two cations given that acetone-ammonia condensation reactions can have many different products.²²

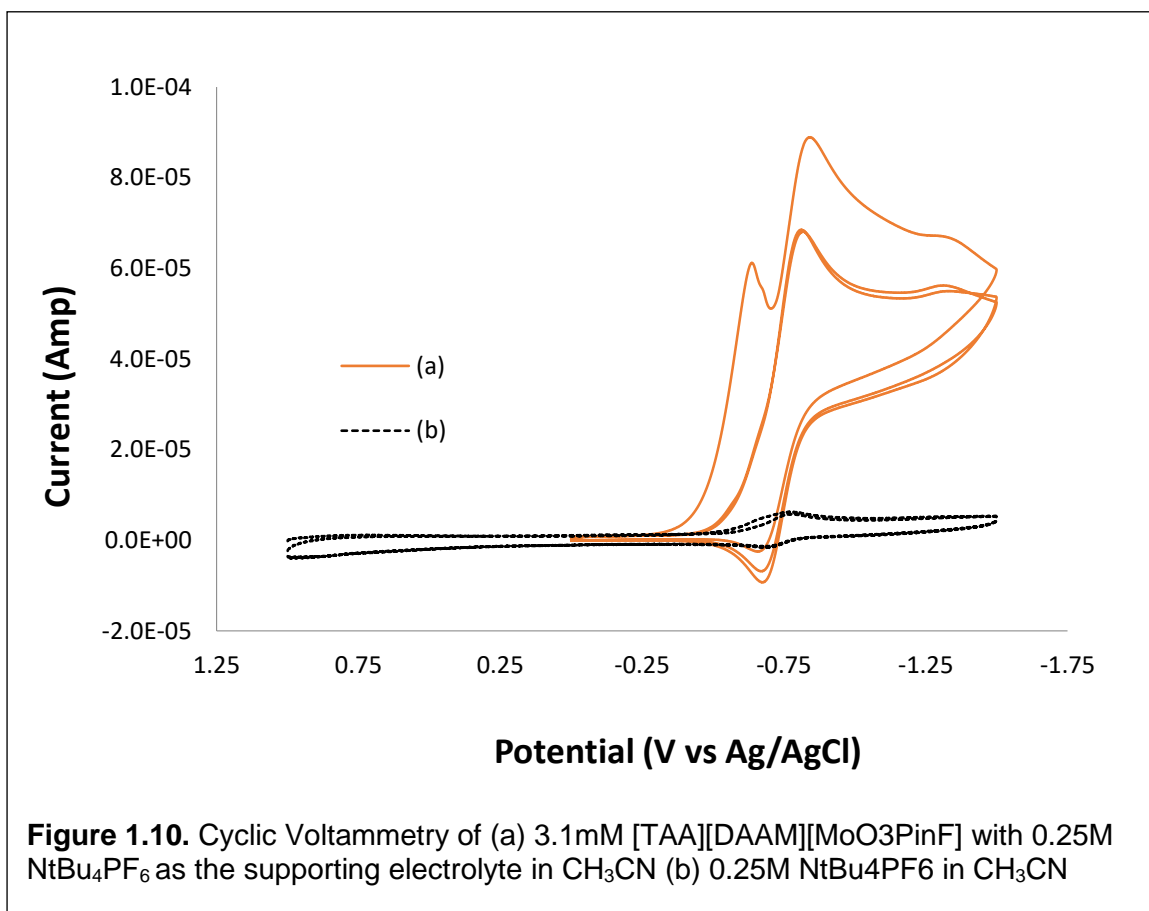




1.3.3 Electrochemistry

Compound **I** was characterized via cyclic voltammetry to understand its electrochemical profile. Three rounds of cyclic voltammetry in a range of 0 to -1.5 V at 100mV/s shows that **I** undergoes an irreversible reduction at -0.63 V and another reduction at -0.84 V (Fig. 1.10). The peak indicating the irreversible reduction is not seen again in subsequent sweeps but the peak at -0.84 V is repeated. The reduction at -0.63 V suggests that a new species is formed, possibly a Mo(V)-pin^F dimer complex like **IV**. Compound **IV** itself is air stable and the crystal structure reveals that it is not a mixture of different Mo-pin^F complexes but purely a Mo(V) dimer. The reduction at -0.84V and oxidation at -0.7V suggest that the molybdenum atom in **I** can reach an oxidation state of Mo(IV), possibly

via another removal of a terminal oxygen or attachment of a proton to the terminal oxygen to create a hydroxyl group. Compound **I** has three doubly-bonded terminal oxo groups attached to the Mo center so further reduction is possible.



1.4 Conclusions and Future Directions

The syntheses of complexes **I - IV** demonstrate that 4*d* transition metals are a new field of viable candidates for investigation in perfluoropinacolate coordination chemistry. Mo is of interest because of its potential as an oxygen atom transfer catalyst, and in olefin epoxidation reactions. Mo-pin^F complexes are air stable and maintain a high oxidation state with multiple Mo=O bonds, which is also a feature of Mo containing enzymes in

nature. The structural data adds to the understanding of coordination difference among metals with different oxidation states.

More chemical features of the Mo-pin^F complexes are potentially amenable to characterization methods such as UV-vis and EPR spectroscopy. Data from these experiments can give an understanding of the electronic structure of Mo at different oxidation states as well as their reactivity to use as catalysts. Further study of the reactivity of **I** – **IV** with various alkenes could lead to their application for catalysis or O-atom transfer.

Further work is needed to find conditions and methods to selectively synthesize **II** and **III** as well as determining the mechanisms that occur during the transition of **II** into **III** and vice versa. Another substance that has not been successfully isolated during the synthesis of **II** and **III** is that of the thin green needles that occurred when an aqueous solution of **II** and **III** in EtOH was heated to boiling point for an hour then cooled down to room temperature. This green color has not been observed before with molybdenum pin^F complexes. This color is indicative of a possibly different oxidation state of molybdenum (**III**).²³ More efforts are required to isolate this substance and determine its chemical identity.

2. Investigation of CuSn Alloys for Nitrate Reduction Catalysis

2.1 Introduction

Algal blooms are a phenomenon that is a global problem and another alarming indicator that the environment is in danger from human activity. When algae flourish so rapidly, they consume a massive amount of oxygen in water that would have otherwise been available for other marine and freshwater living organisms to sustain life. Death of ecosystems is detrimental to humans as well because contaminated fresh water or polluted harvest from the sea can negatively affect human health. Algal blooms happen because of the presence of excessive nutrients in water. One of the nutrients that lets algae thrive is nitrate (NO_3^-). Nitrate accumulates in excessive amounts in surface waters and underground reservoirs as the aftermath of the development of the Haber-Bosch process. This discovery of a method to produce ammonia (NH_3), via catalysis by iron, on an industrial scale made mass production of nitrogen-based fertilizers possible.²⁴ As living organisms utilize the nitrogen atom in NH_3 to synthesize necessary amino acids through a process of nitrification, the byproduct, NO_3^- , is also released back into open water.²⁵ The abundant use of fertilizer in agriculture led to NO_3^- accumulation in water, which in turn, led to algal blooms.

As the algal bloom phenomenon persisted and continued to harm the environment, many efforts were put into reverse the accumulation of NO_3^- . One method that has attracted considerable attention is electrocatalytic reduction.²⁶ Ideally, in this process NO_3^- would be reduced back to N_2 , which is inert, and is attractive because other nitrogen species such as NO and NO_2^- are both environmentally hazardous. Previously in the Doerr group, the complex $\text{K}_2[\text{Cu}(\text{pin}^{\text{F}})_2]$ was studied as a pre-catalyst in the reduction of NO_3^- . It was discovered that Cu(II) is reduced to Cu(0) before Cu can catalyze the reduction of NO_3^- and that the end product of the reduction is primarily NH_3 .²⁷

A second metal, Sn , forms an alloy with Cu in a basic pH environment and was

also studied because of its potential to catalyze the reduction of NO_3^- to N_2 .^{28,29} Selectivity towards N_2 over NH_3 as the final product is also desired because NH_3 is a greenhouse gas, and additional algal nutrient, despite its important use in industry. Using Cu and Sn as a co-catalyst in bulk together in a neutral pH is an experiment with promising potential. Cu is very efficient in NO_3^- reduction but the primary end-product is NH_3 . Whereas Sn is not as efficient as Cu in the initial NO_3^- reduction step in the series of nitrogen species reduction, Sn does have the important advantage of promoting the production of N_2 over NH_3 . The goal of using Cu and Sn combined is to see if the desirable traits of each metal are preserved. Ideally, a NO_3^- reduction catalyst should have good efficiency and selectivity towards N_2 production.

2.2 Experimental

2.2.1 General Procedures

All starting materials were commercially available and used without further purification. Stock solutions of KCl, KNO_3 , NaNO_2 , H_2SO_4 , HCl were prepared to serve as supporting electrolytes or reagents for electrochemistry experiments. Measurements of electrochemistry data were collected using a three-electrode cell connected to an external CHI 630C potentiostat run by a personal computer with CHI software. A glassy carbon electrode (GCE) (0.5 mm diameter) was employed as the working electrode, with Ag/AgCl electrode as the reference electrode and Pt wire as the counter electrode, respectively. The working electrode was cleaned between experiments using 5 μm Al_2O_3 suspended in water, a polishing pad and carefully dried. All potentials are reported *versus* [Ag]⁺/[AgCl]. Absorbance was measured by a Molecular Devices SpectraMax M5 Multimode Microplate reader with Softmax Pro V5 software. SEM experiments were conducted using a Zeiss

SUPRA 55VP Field Emission Scanning Electron Microscope, operating at 5 kV. The microscope is completely controlled from a computer workstation. The electron source is a thermal field emission gun (Schottky type). Images were created using the SMARTSEM software.

2.2.2 Linear Sweep Voltammetry (LSV)

Following deposition of Cu:Sn materials on GCEs, LSV was conducted in the direction of increasing potential in a range of scan rate from 0.01 to 0.05 V/s starting from potential as low as -1.5 V to potential as high as 1.5 V. Potential was sampled at an interval of every 0.001 V. The experiment was run in a 50mM solution of KCl in water degassed with N₂ for 10 min.

2.2.3 Cyclic Voltammetry (CV)

CV was conducted starting from a potential as high as +1 V toward the direction of a decreasing potential to as low as -2 V and returned back to the starting potential. This cycle was repeated two more times which makes the total number of sweeps to be six. Scan rate was 0.100 V/s and the current value was sampled at an interval of every 0.001 V. The solutions used to run CV were a mixture 50mM of KCl and 50mM of KNO₃ in water and another mixture of 50mM KCl and 50mM of NaNO₂ in water. A glassy carbon electrode (GCE) was used as the working electrode for metal deposition and the current value was measured as the applied potential changed. A catalytic response is detected if a sudden current increase is seen during the reductive scan.

2.2.4 Controlled Potential Electrolysis (CPE)

CPE experiments to deposit metal on the GCE were conducted at -0.6 V for 60 seconds. The solutions CPE for deposition used were 1M H₂SO₄ or 1M HCl with varying amount of CuCl₂ and SnCl₂ that were degassed with N₂ for 10 min. CPE was used later to determine the amount of deposition via LSV using 10mM SnCl₂ 10mM CuCl₂ in 1M H₂SO₄ or 1M HCl. CPE to deposit metal or metal alloys for later use as catalysts for NO₃⁻ reduction used varying amounts of CuCl₂ and SnCl₂ whose concentrations ranged from 1 mM to 10 mM. CPE experiments to reduce NO₃⁻ were conducted at -1.1 V for 180 min. Samples were collected at 0, 30, 60, 120, 180 min after the start of the experiment. The solutions used to run CPE for NO₃⁻ reduction were 50mM KCl in water with varying amount of KNO₃ ranging from 2.5 to 5mM.

2.2.5 Microcolorimetric Assay

All microcolorimetric methods were adapted from published procedures.^{30,31} Standard solutions of NH₄Cl, NaNO₂, and KNO₃ with concentrations 1, 2, 5, 10, 20, 50, 100 μM were prepared for each chemical respectively with water. Each species used a separate 96 well clear flat-bottomed microplate. A standard solution of each concentration and collected samples from CPE experiments occupied three wells each. The average absorbance value of the standard solution with known concentration was then used to find a linear relationship between concentration of the nitrogen species of interest and absorbance value. This calibration is used to determine the unknown nitrogen species concentration of the collected samples.

For the NO₂⁻ quantification assay, a reagent that detected NO₂⁻ was prepared by mixing 50μL of 58 mM sulfanilamide in 3.6 M HCl and 50 μL of 3.9 mM N-(1-

naphthyl)ethylenediamine (NEDD). This reagent was then added to 100 μL of the standard solution and samples inside the microplate well, vortexed for 30 min at 900 rpm then measured for absorbance at 540nm. NO_2^- is detected visibly as red purple in intensity proportional to concentration.

NO_3^- assays use the same reagents as the NO_2^- assays with an additional reducing agent introduced by adding 10mL of solution of 6mM VCl_3 , 0.5M HCl to 10mL of 0.12M sulfanilamide, 4mM NEDD, 0.5M HCl. This 150 μL reducing reagent added to each well converts NO_3^- in the 150 μL of standard or collected to NO_2^- which in turn reacts with the reagent. The microplate for NO_3^- is kept in dark for at least 6 hours before absorbance is measured at 540nm.

NH_3 assay uses 3 reagents, the first one being 1632 mM citric acid in water. 10 μL of the first reagent is added to 200 μL of standard or sample then vortexed for 2 min at 750 rpm. The second reagent is 404 mM Phenol in 1.3 mM sodium nitroprusside dihydrate in water. 10 μL of the second reagent is added then vortexed again for 2 min at 750 rpm. The third reagent is prepared by dissolving 0.2 g sodium hydroxide in 200 μL sodium hypochlorite solution then adding water to make the final volume 10 mL. 10 μL of the third reagent is added to the wells and the microplate is vortexed again for 2 min at 750 rpm. NH_3 is detected as bright blue and absorbance is measured at 630 nm.

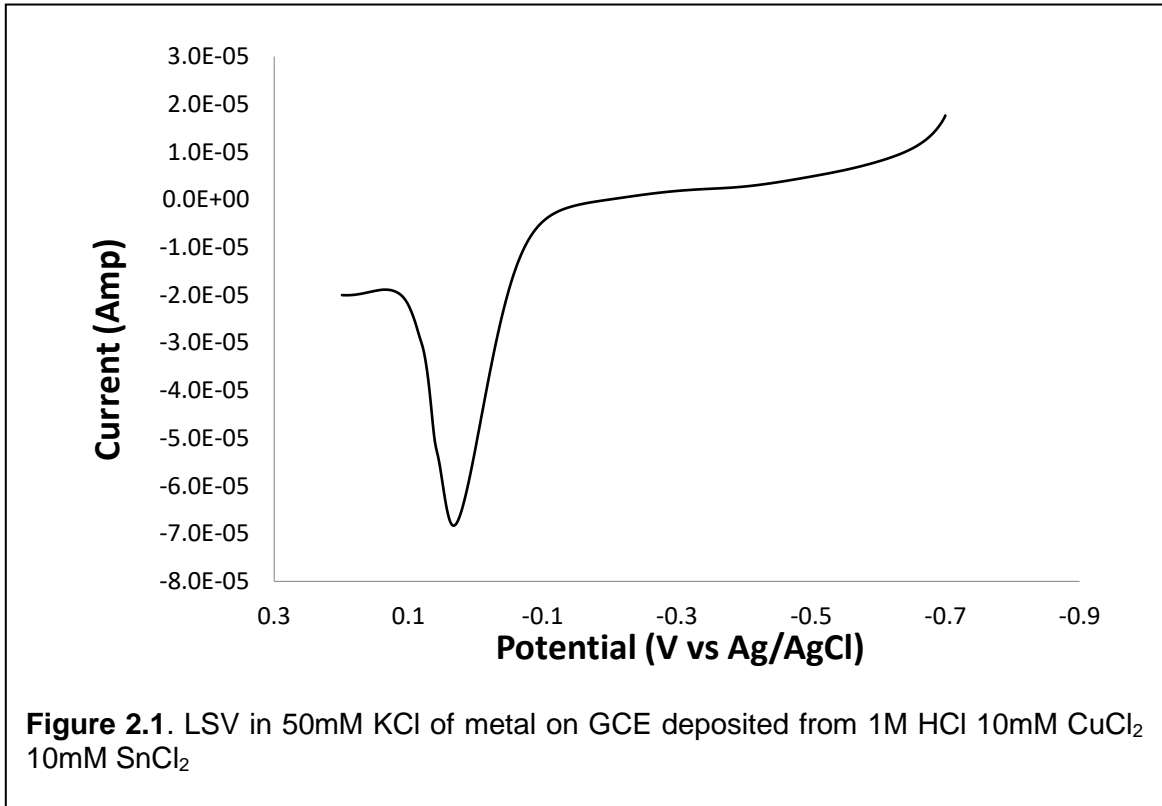
2.3 Results and discussion

2.3.1 Linear Sweep Voltammetry

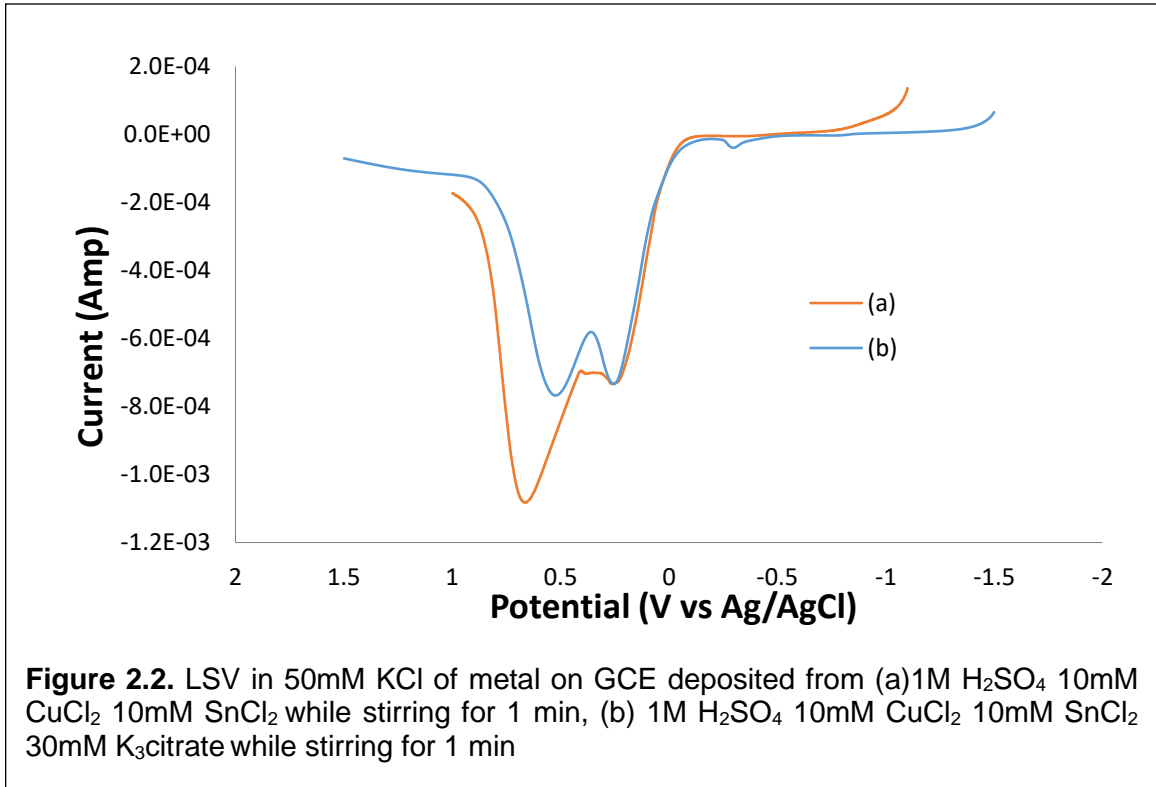
LSV is an indirect method to measure metal deposition on a GCE. As the deposited metal re-oxidizes and diffuses back into solution, current is generated which is quantified by the potentiostat.

The first method to deposit Cu and Sn was an ion exchange method in which due to the difference in oxidation potential, Cu^{2+} would displace already deposited Sn(0) on the GCE surface and take its place as it is reduced to Cu(0) with the concomitant oxidation of Sn to Sn(II). LSV results from this method show that the deposition of Cu or Sn is miniscule and it is hard to determine if the current peaked at all. The amount of current is very small compared to subsequent results from different methods and this approach was consequently abandoned.

A second method of obtaining Cu-Sn materials involving the co-deposition of both metals concurrently was also attempted. CPE was conducted with a solution with an equimolar ratio of Cu and Sn (both 10mM) before conducting an LSV. In this case, the LSV current has a peak value of -7×10^{-7} Amp (Fig. 2.1). Despite detecting an increase in current, the metal deposition prepared by this method did not show catalytic reduction of NO_3^- .



Changing the method to include stirring the solution while running CPE for deposition results in a larger peak value during LSV. Co-deposition of 10 mM CuCl₂ 10 mM SnCl₂ 0.1M H₂SO₄ with stirring, the peak current is -1.1×10^{-3} Amp (Fig 2.2). Furthermore, the addition of 30 mM K₃citrate as a surfactant during deposition also yields large peak during LSV at -8×10^{-4} Amp (Fig 2.2). Deposition of Cu and Sn while stirring the solution is reasonable because, with the metal ions in constant motion, a greater number of ions can have contact with the GCE surface and become reduced.



2.3.2 Cyclic Voltammetry

Cyclic voltammetry was conducted using metal deposition with varying ratios of Cu and Sn in the starting solution. Each combination of varying amounts of Cu and Sn deposited on the GCE was used in the subsequent CVs in solutions with NO₃⁻ or NO₂⁻. As more Sn was added, the reduction peak of NO₃⁻ reduction was more negative (see Table 2.1), requiring more electrochemical energy. The maximum current measured at -1.2V for each case differed. NO₃⁻ reduction with only Cu had the highest maximum current. Out of the different combinations of Cu and Sn, the deposition with Cu to Sn ratio of 1:1 had the highest maximum current. Sn by itself did not have catalytic reduction of NO₃⁻. This demonstrates that using Sn with Cu can maintain the catalytic effect of Cu despite requiring more energy and having lesser efficiency. Also noticeable is that during the

oxidative sweep in a CV, Cu and Sn deposits were re-oxidized into solution, leaving less metal to act as a catalyst with each subsequent sweep.

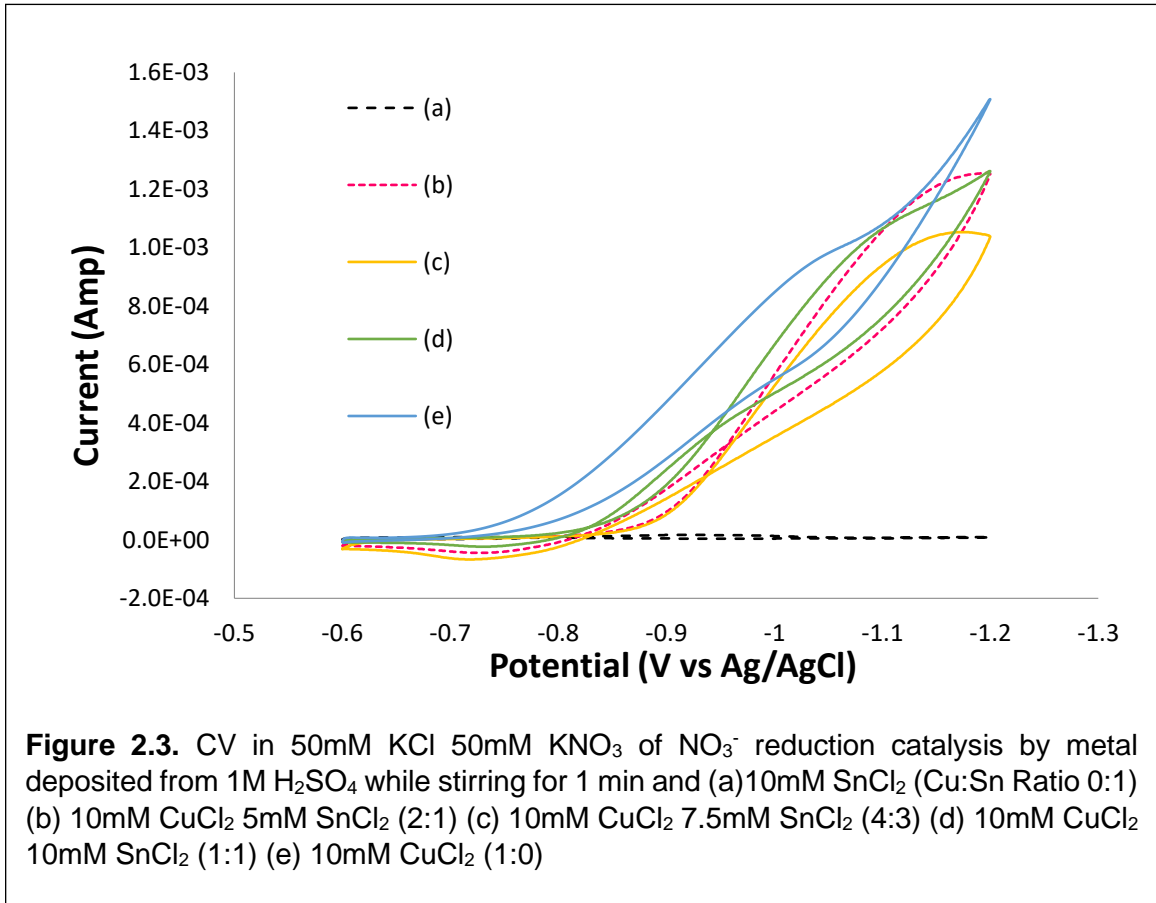
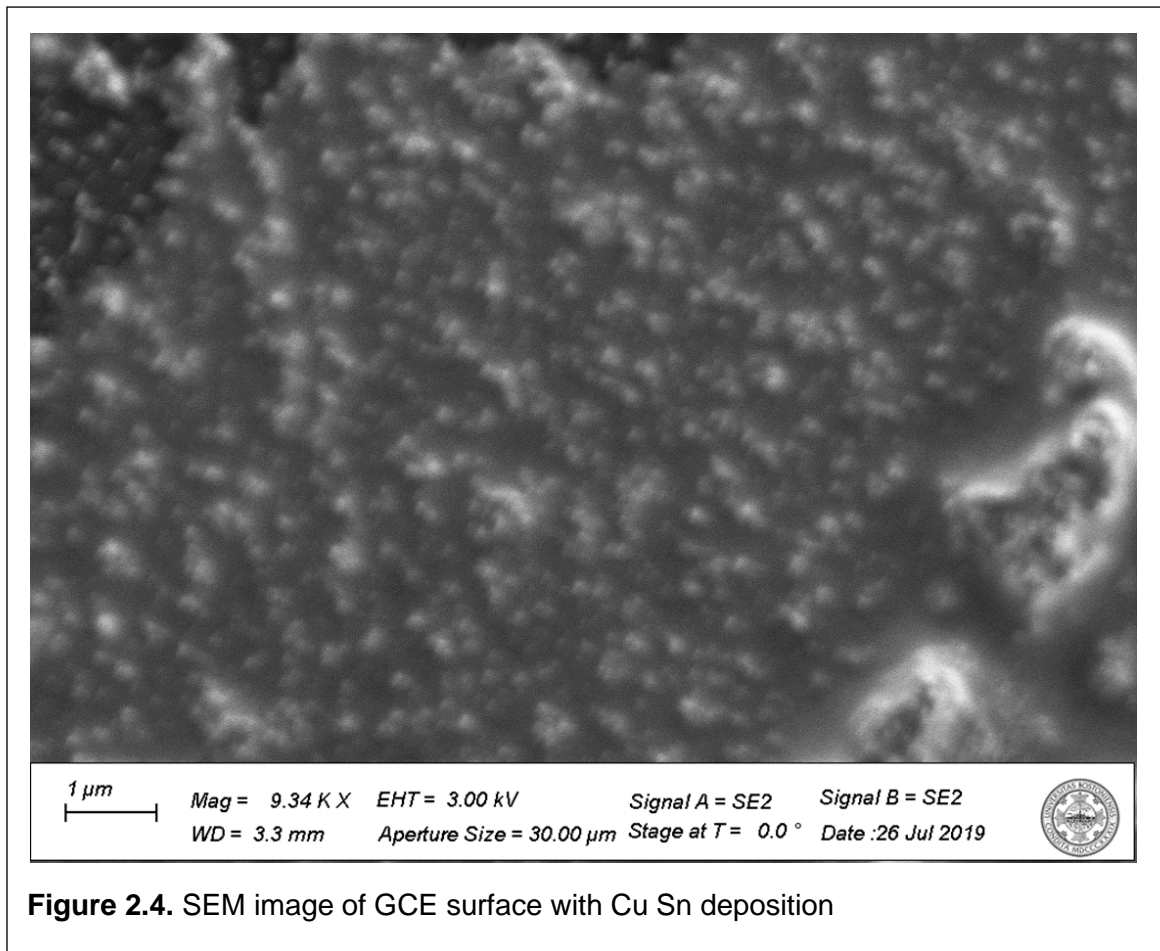
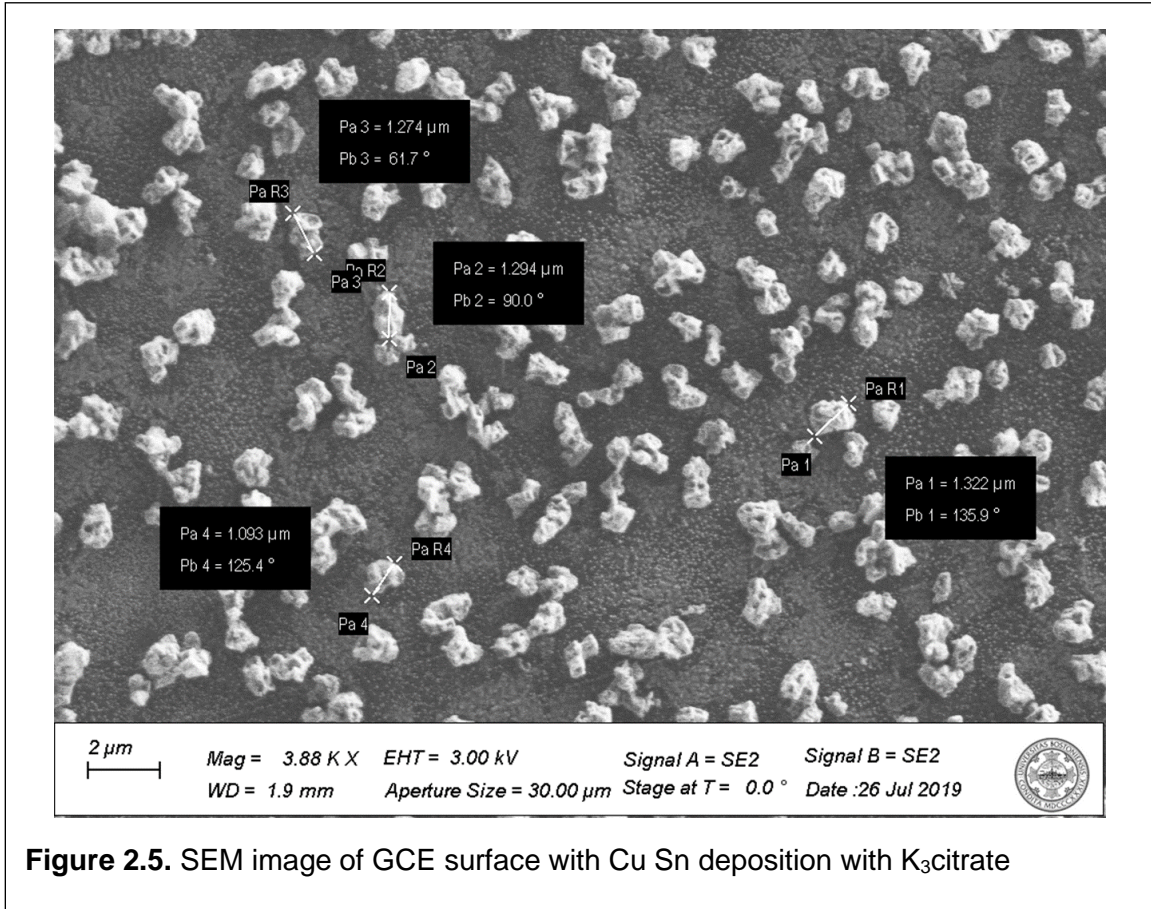


Table 2.1. Potential of Reduction Peak of NO₃⁻ Reduction and Current at -1.2V Based on Cu Sn Ratio

Cu:Sn Ratio	Potential of Reduction Peak (V)	Current at -1.2V (Amp)
0:1	No Catalysis	9.46E-06
2:1	-1.17	0.001253
4:3	-1.17	0.001038
1:1	-1.13	0.001262
1:0	-1.04	0.001508

The re-oxidation of Cu and Sn was not seen when K_3 citrate was included as a surfactant during the deposition. The presence of bulky and negatively charged citrate in solution could possibly promote metal ions to attach to the GCE surface in a more uniform manner while also stabilizing the deposits. A scanning electron microscopy (SEM) images of the GCE surface (Figs. 2.4 and 2.5) comparing the effect of the K_3 citrate additive (Fig. 2.5) shows that Cu and Sn deposits are more uniform in size and similarly shaped whereas in the case of no added K_3 citrate (Fig 2.4), Cu and Sn are highly amorphous. Whether or not physical morphology affects the stability and reactivity of Cu and Sn metals is an area for further investigation.





CV results for NO_2^- reduction were challenging to draw conclusions from. Additional factors other than re-oxidation of Cu and Sn exist. Namely, when a more negative potential is applied hydrogen gas evolution occurs at potential lower than -1.45V.^{32,33} As protons are drawn to the GCE cathode and are reduced, they leave the solution as H_2 gas. Subsequently, Cu and Sn deposits break off mechanically and are thus unable to function as a catalyst once the alloy loses contact with the GCE surface. One important observation is that as the Sn content increases, fewer bubbles were observed. A CV with only Sn deposition withstood low potentials without noticeable loss from the GCE. With more Cu, the amount of H_2 gas evolving and the amount of detachment of the

deposited metal increased. Further work to find the ratio of Cu and Sn that is stable in low potentials and also has catalytic effect is warranted.

2.3.3 *Microcolorimetric Assay*

A microcolorimetric assay is a useful method to quantify very small amounts, for example 1 μM , of a chemical species of interest. When used with samples collected from CPE, it is possible to assess the catalytic effect of Cu and Sn by analyzing the nitrogen species left in the solution both during and following electrolysis. The results of the assay data are not presented here due to issues with the irreproducibility of the microcolorimetric assays. Further optimization is required to prepare the standard and reagents in a timely manner before NO_2^- reverts back to NO_3^- with abundant source of oxygen in the air. Additionally, NH_3 is a volatile gas, and with enough time, gaseous NH_3 can migrate to other wells in the microplate causing a false positive result.

2.4 Conclusions and Future Directions

This preliminary work shows that Cu and Sn are candidates to consider for catalysis of NO_3^- reduction. Deposition of Cu and Sn on a GCE to form an alloy that can catalyze NO_3^- reduction significantly is possible with the addition of stirring during deposition. Moreover, the addition of $\text{K}_3\text{citrate}$ as a surfactant causes a more uniform deposition and appears to increase the stability of the deposited material as Cu and Sn materials prepared in this manner are more resistant to re-oxidation during CV experiments. However, more work is required to determine the relationship between the CuSn-alloy morphology and stability. One challenge that must be addressed in future studies is how to minimize the H_2 evolution that occurs at low potentials, and mechanically breaks up surface deposits. Another

important challenge in this work is the quantitative (and qualitative) analysis of the reduction products. To this end, the development of a reproducible method of preparing microcolorimetric assays would be a of great benefit.

References

- (1) G. Caulton, K.; G. Hubert-Pfalzgraf, L. Synthesis, Structural Principles and Reactivity of Heterometallic Alkoxides. *Chemical Reviews* **2002**, *90* (6), 969–995. <https://doi.org/10.1021/cr00104a003>.
- (2) Grass, A.; Wannipurage, D.; Lord, R. L.; Groysman, S. Group-Transfer Chemistry at Transition Metal Centers in Bulky Alkoxide Ligand Environments. *Coordination Chemistry Reviews* **2019**, *400*, 213044. <https://doi.org/10.1016/J.CCR.2019.213044>.
- (3) Willis, C. J. Fluorinated Alcohols and Their Metal Complexes. *Coordination Chemistry Reviews* **1988**, *88*, 133–202. [https://doi.org/10.1016/0010-8545\(88\)80003-1](https://doi.org/10.1016/0010-8545(88)80003-1).
- (4) Brazeau, S. E. N.; Doerrler, L. H. Cu(i)-O₂ Oxidation Reactions in a Fluorinated All-O-Donor Ligand Environment. *Dalton Transactions*. Royal Society of Chemistry 2019, pp 4759–4768. <https://doi.org/10.1039/c8dt05028g>.
- (5) Elinburg, J. K.; Carter, S. L.; Nelson, J.; Fraser, D. G.; Beeler, A. B.; Nordlander, E.; Rheingold, A.; Doerrler, L. H. Reversible H-Atom Transfer and Catalytic Oxidative Alcohol Dehydrogenation by Vanadyl Perfluoropinacolate Complexes. *Unpublished Work* **2019**.
- (6) Steele, J. L.; Tahsini, L.; Sun, C.; Elinburg, J. K.; Kotyk, C. M.; McNeely, J.; Stoian, S. A.; Dragulescu-Andrasi, A.; Ozarowski, A.; Ozerov, M.; Krzystek, J.; Telser, J.; Bacon, J. W.; Golen, J. A.; Rheingold, A. L.; Doerrler, L. H. Square-Planar Co(III) in {O₄} Coordination: Large ZFS and Reactivity with ROS. *Chemical Communications* **2018**, *54* (85), 12045–12048. <https://doi.org/10.1039/c8cc04464c>.
- (7) Cantalupo, S. A.; Fiedler, S. R.; Shores, M. P.; Rheingold, A. L.; Doerrler, L. H. High-Spin Square-Planar Co II and Fe II Complexes and Reasons for Their Electronic Structure. *Angewandte Chemie - International Edition* **2012**, *51* (4), 1000–1005. <https://doi.org/10.1002/anie.201106091>.
- (8) Zheng, B.; O. Miranda, M.; G. DiPasquale, A.; A. Golen, J.; L. Rheingold, A.; H. Doerrler, L. Synthesis and Electronic Spectra of Fluorinated Aryloxide and Alkoxide [NiX₄]²⁻ Anions. *Inorganic Chemistry* **2009**, *48* (10), 4274–4276. <https://doi.org/10.1021/ic9003593>.
- (9) Tahsini, L.; Specht, S. E.; Lum, J. S.; Nelson, J. J. M.; Long, A. F.; Golen, J. A.; Rheingold, A. L.; Doerrler, L. H. Structural and Electronic Properties of Old and New A₂[M(PinF)₂] Complexes. *Inorganic Chemistry* **2013**, *52* (24), 14050–14063. <https://doi.org/10.1021/ic401837y>.

- (10) CRC Handbook of Chemistry and Physics. *Chemical Rubber Company handbook of chemistry and physics*. Electronic. Boca Raton, Fla.: CRC Press : Taylor & Francis: Boca Raton, Fla. 1970.
- (11) Hille, R., Hall, J., Basu, P. The Mononuclear Molybdenum Enzymes. *Chemical Reviews* **2014**, *114* (7), 3963–4038. <https://doi.org/10.1021/cr400443z>
- (12) Raybaud, P.; Hafner, J.; Kresse, G.; Kasztelan, S.; Toulhoat, H. Ab Initio Study of the H₂-H₂S/MoS₂ Gas-Solid Interface: The Nature of the Catalytically Active Sites. *Journal of Catalysis* **2000**, *189* (1), 129–146. <https://doi.org/10.1006/jcat.1999.2698>.
- (13) Acharya, S.; Hanna, T. A. Epoxidation of Alkenes Catalyzed by Some Molybdenum(0) and Molybdenum(IV) Complexes. *Polyhedron* **2016**, *107*, 113–123. <https://doi.org/10.1016/j.poly.2016.01.022>.
- (14) Schurig, V.; Hintzer, K.; Leyrer, U.; Mark, C.; Pitchen, P.; Kagan, H. B. *Enantioselective Epoxidation of Unfunctionalized Simple Olefins by Non-Racemic Molybdenum(VI) (Oxo-Diperoxo) Complexes*; Elsevier Sequoia S.A, 1989; Vol. 370.
- (15) Sheldon, R. A.; van Doorn, J. A. Metal-Catalyzed Epoxidation of Olefins with Organic Hydroperoxides I. A Comparison of Various Metal Catalysts. *Journal of Catalysis* **1973**, *31* (3), 427–437. doi: 10.1016/0021-9517(73)90314-x
- (16) Ameh, E. S. A Review of Basic Crystallography and X-Ray Diffraction Applications. *International Journal of Advanced Manufacturing Technology* **2019**, *105* (7–8), 3289–3302. <https://doi.org/10.1007/s00170-019-04508-1>.
- (17) Roberts, J. D. Nuclear Magnetic Resonance Spectroscopy. *Journal of Chemical Education* **1961**, *37*, 581–585.
- (18) Arnhiz, F. J. Microscale Synthesis of MoO₂(Acac)₂. *Journal of Chemical Education* **1995**, *72*, A7–A8.
- (19) Chen, Q.; Ma, L.; Liu, S.; Zubieta, J. Structural Characterization of the Pentamolybdate Anion, [(MoO₄)₂{Mo₃O₈(OMe)}]₃⁻, and Isolation of the [Mo₃O₈(OMe)]⁺Trinuclear Core in the Squarate Complex [{Mo₃O₈(OMe)}(C₄O₄)₂]₃. *Journal of the American Chemical Society* **1989**, *111* (15), 5944–5946. <https://doi.org/10.1021/ja00197a067>.
- (20) C. Buzzeo, M.; H. Iqbal, A.; M. Long, C.; Millar, D.; Patel, S.; A. Pellow, M.; A. Saddoughi, S.; L. Smenton, A.; F. C. Turner, J.; D. Wadhawan, J.; G. Compton, R.; A. Golen, J.; L. Rheingold, A.; H. Doerrer, L. Homoleptic Cobalt and Copper Phenolate A₂[M(OAr)₄] Compounds: The Effect of Phenoxide Fluorination. *Inorganic Chemistry* **2004**, *43* (24), 7709–7725. <https://doi.org/10.1021/ic0493954>.

- (21) Matheson, A. J.; Penfold, B. R. $\{\mu\}$ -Oxo-Bis{[2,3-Dimethyl-2,3-Butanediolato(1-)] [2,3-Dimethyl-2,3-Butanediolato(2-)] Oxomolybdenum(VI)}. *Acta Crystallographica Section B* **1979**, 35 (11), 2707–2709. <https://doi.org/10.1107/S0567740879010268>.
- (22) Gliozzi, G.; Frattini, L.; Righi, P.; Cavani, F. Towards a More Sustainable Production of Triacetoneamine with Heterogeneous Catalysis. *Journal of Molecular Catalysis A: Chemical* **2014**, 393, 325–332. <https://doi.org/10.1016/j.molcata.2014.06.023>.
- (23) G. Stark, J. The Oxidation States of Molybdenum. *Journal of Chemical Education* **1969**, 46 (8). <https://doi.org/10.1021/ed046p505>.
- (24) Cherkasov, N.; Ibhaddon, A. O.; Fitzpatrick, P. A Review of the Existing and Alternative Methods for Greener Nitrogen Fixation. *Chemical Engineering and Processing: Process Intensification* **2015**, 90, 24–33. <https://doi.org/10.1016/j.cep.2015.02.004>.
- (25) Rosca, V.; Duca, M.; DeGroot, M. T.; Koper, M. T. M. Nitrogen Cycle Electrocatalysis. *Chemical Reviews* **2009**, 109 (6), 2209–2244. <https://doi.org/10.1021/cr8003696>.
- (26) Garcia-Segura, S.; Lanzarini-Lopes, M.; Hristovski, K.; Westerhoff, P. Electrocatalytic Reduction of Nitrate: Fundamentals to Full-Scale Water Treatment Applications. *Applied Catalysis B: Environmental* **2018**, 236, 546–568. <https://doi.org/10.1016/J.APCATB.2018.05.041>.
- (27) Hannigan, S. F. Redox Reactions of Copper Complexes with Fluorinated Oxygen-Donating Ligands. Doctoral dissertation – Boston University, 2017. <https://open.bu.edu/handle/2144/27073>
- (28) MácOva, Z.; Bouzek, K.; Šerak, J. Electrocatalytic Activity of Copper Alloys for NO₃⁻ Reduction in a Weakly Alkaline Solution : PPPart 2: Copper-Tin. *Journal of Applied Electrochemistry* **2007**, 37 (5), 557–566. <https://doi.org/10.1007/s10800-006-9287-8>.
- (29) Tada, K.; Shimazu, K. Kinetic Studies of Reduction of Nitrate Ions at Sn-Modified Pt Electrodes Using a Quartz Crystal Microbalance. *Journal of Electroanalytical Chemistry* **2005**, 577 (2), 303–309. <https://doi.org/10.1016/J.JELECHEM.2004.11.039>.
- (30) Ringuet, S.; Sassano, L.; Johnson, Z. I. A Suite of Microplate Reader-Based Colorimetric Methods to Quantify Ammonium, Nitrate, Orthophosphate and Silicate Concentrations for Aquatic Nutrient Monitoring. *Journal of Environmental Monitoring* **2011**, 13 (2), 370–376. <https://doi.org/10.1039/c0em00290a>.

- (31) Doane, T. A.; Horwáth, W. R. Spectrophotometric Determination of Nitrate with a Single Reagent. *Analytical Letters* **2003**, 36 (12), 2713–2722.
<https://doi.org/10.1081/AL-120024647>.
- (32) Reyter, D.; Bélanger, D.; Roué, L. Study of the Electroreduction of Nitrate on Copper in Alkaline Solution. *Electrochimica Acta* **2008**, 53 (20), 5977–5984.
<https://doi.org/10.1016/J.ELECTACTA.2008.03.048>.
- (33) Farinazzo Bergamo Dias Martins, P.; Papa Lopes, P.; Ticianelli, E. A.; Stamenkovic, V. R.; Markovic, N. M.; Strmcnik, D. Hydrogen Evolution Reaction on Copper: Promoting Water Dissociation by Tuning the Surface Oxophilicity. *Electrochemistry Communications* **2019**, 100, 30–33.
<https://doi.org/10.1016/J.ELECOM.2019.01.006>.

Curriculum Vitae

